COMPDYN 2009
ECCOMAS Thematic Conference on
Computational Methods in Structural Dynamics and Earthquake Engineering
M. Papadrakakis, N.D. Lagaros, M. Fragiadakis (eds.)
Rhodes, Greece, 22–24 June 2009

INTERACTION OF A LINED TUNNEL WITH THE SURROUNDING NON-LINEAR GROUND DUE TO A VERTICAL SHEAR WAVE

J. R. Maranha[1] **and A. Vieira**[1]

[1] Civil Engineering National Laboratory (LNEC)
Av. do Brasil, 101, Lisboa, Portugal
e-mail: {jmaranha,avieira}@lnec.pt

Keywords: Earthquake Engineering, Soil Mechanics, Tunneling.

Abstract. *When analysing the effects of seismic actions on lined tunnels, a non-linear soil model able to reproduce the main features of cyclic behaviour, such as damping and pore pressure generation, should be used. In this work, a horizontal shear wave propagating upwards corresponding to a constant amplitude spectral acceleration in a bandwidth limited frequency domain interacts with a lined tunnel, excavated in saturated overconsolidated hard clay. Initial values of the model's internal variables consistent with an overconsolidated initial stress field including the tunnel's construction effect are considered. Different amplitudes of the input signal are applied. Both a bounding surface "bubble" model, proposed by Kavvadas and Belokas [1] for structured overconsolidated soils with anisotropy, and a hysteretic model included in the software FLAC are used for the soil.*

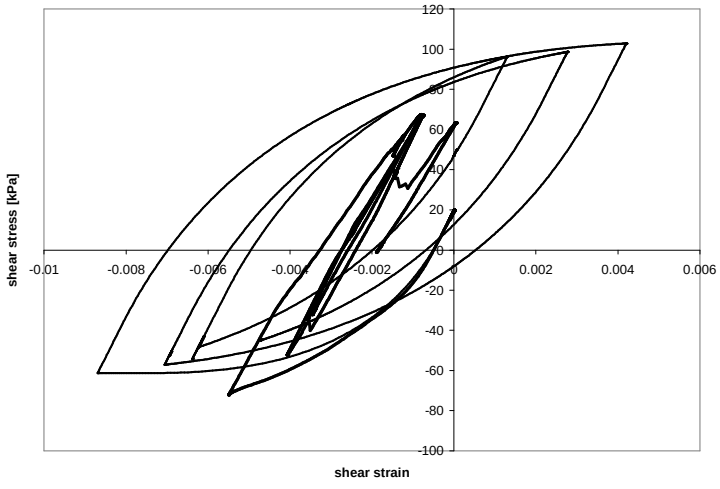

1 INTRODUCTION

The analysis of the response of geotechnical structures to cyclic loading requires the use of sophisticated material models. In this work, the analysis of a tunnel, excavated in overconsolidated clay, submitted to a seismic loading having constant spectral amplitude and limited bandwidth is presented.

Two different non-linear soil models having different degrees of complexity were used and three acceleration histories with increasing amplitude were applied. The response at some points in the model is presented in the form of spectral acceleration amplification ratios, stress-strain curves, pore pressure and relative displacement histories.

2 MODELS' DESCRIPTION

2.1 The bounding surface bubble model

The model adopted here was formulated by Kavvadas and Belokas [1]. It is a generalisation of the Modified Cam-Clay Model (MCCM), with continuous plasticity, following the general bounding surface formulation of Dafalias [2]. The bounding surface is a sheared ellipsoid (see Figure 1), which makes the plastic behaviour anisotropic. The model includes a mechanism to simulate the strain induced destructuring, which is a relevant aspect of natural soils.

The most exterior surface, the bounding surface, which is the Structure Strength Envelope (SSE), represents the material with its structure intact, and is defined by the function:

$$\mathrm{F}(\boldsymbol{\sigma},\boldsymbol{\sigma}_K,\alpha)=\frac{1}{c^2}\left(\mathbf{s}-\frac{p}{p_K}\mathbf{s}_K\right):\left(\mathbf{s}-\frac{p}{p_K}\mathbf{s}_K\right)+(p-p_K)^2-\alpha^2=0 \tag{1}$$

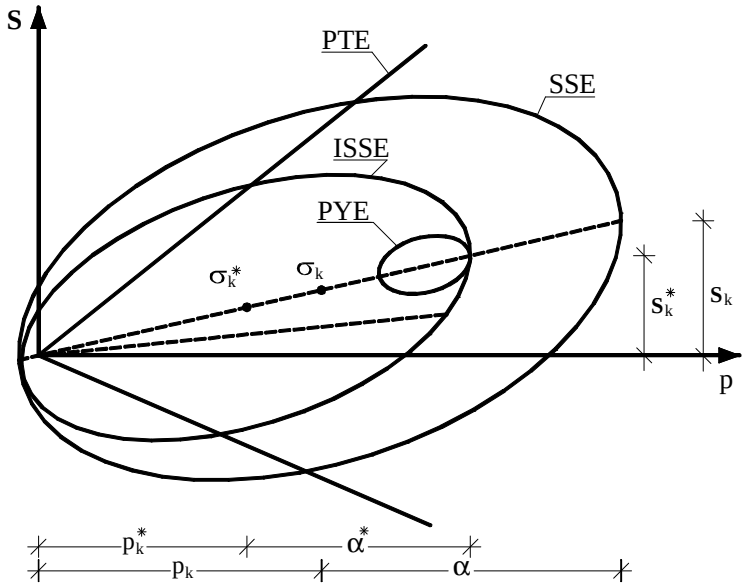

Figure 1: 2D representation of bounding surface model various surfaces.

that, in geometrical terms, describes a sheared ellipsoid of revolution, whose position and alignment is given by the tensor $\boldsymbol{\sigma}_K=\mathbf{s}_K+p_K\mathbf{I}$. The length of the surface in the p axis direc-

tion is 2α. The semi-axis ratio of the ellipsoid depends on the constant c. When $\boldsymbol{\sigma}_K = \alpha \mathbf{I}$ and $c = \sqrt{2/3}\,M$, the Modified Cam-Clay Model's ellipsoid, which is isotropic, is obtained. The interior bubble, that bounds the elastic domain, is the Plastic Yield Envelope (PYE). It is defined, in stress space by the following function:

$$\mathrm{f}\left(\boldsymbol{\sigma}, \boldsymbol{\sigma}_K, \boldsymbol{\sigma}_L, \alpha\right) = \frac{1}{c^2}\left(\mathbf{s} - \mathbf{s}_L - \frac{p - p_L}{\mathrm{p}_K}\mathbf{s}_K\right) : \left(\mathbf{s} - \mathbf{s}_L - \frac{p - p_L}{p_K}\mathbf{s}_K\right) + (p - p_L)^2 - (\xi\alpha)^2 = 0 \quad (2)$$

This PYE bubble is homothetic to the SSE shrunk by a scale factor ξ <<1 and translated $\boldsymbol{\sigma}_L - \boldsymbol{\sigma}_K$ in relation to $\boldsymbol{\sigma}_K$. The PYE, f = 0, is obtained from the SSE substituting $\boldsymbol{\sigma}$ by $\boldsymbol{\sigma} - \boldsymbol{\sigma}_L + \boldsymbol{\sigma}_K$ and α by $\xi\alpha$, in F=0. The tensor $\boldsymbol{\sigma}_L$ is the centre of the bubble (PYE).

The model was implemented into a finite difference code and applied to a tunnel excavation by Maranha and Vieira [3]. In this reference, a description of all model details as well as the meaning of all its material constants can be found.

The material model constants used here were taken from Vallerica clay [4]: B_0=12500kPa, G_0=9375kPa, p_r=100kPa, m=1, λ^*=0.118, κ^*=0.012, n=2, N_{iso}=2.15, Γ=2.08, v_0=1.363, c=0.85, ξ=0.08, k=0.85, p_K=α=500kPa, χ=1, ψ=0, γ=10, λ_1=0.22 and $\hat{\boldsymbol{\xi}} = 0$. Load induced anisotropy and destructuring were not considered (ψ=0) and as such the associated constants are zero.

2.2 Hysteretic model available in the FLAC code

The hysteretic model implemented in the FLAC code is a nonlinear model in which both the bulk, K, and the shear, G, moduli are shear strain dependent. The model also incorporates the Masing rules for cyclic loading. Damping arises from the closed hysteretic loops. Also, because volumetric behaviour is independent of the shear one, dilatancy cannot be represented.

In order to be able to compare both models, a procedure for the adjustment of the shear modulus reduction (with shear strain) curves was undertaken. For the bubble model, an initial isotropic effective stress of 300kPa was used. This corresponds approximately to the stress acting at the tunnels midsection level before excavation. The curve of the hysteretic model (adjusted to the bubble model), together with the one from the bubble model, are presented in Figure 2. The initial elastic constants of the bubble model were used in the hysteretic model. The two parameters of the default FLAC hysteretic model were L_1=-1.2 and L_2=0.9.

In theory, the elastic domain (the "bubble") can be as small as desired. However, it has been observed that, if the size of the bubble is too small, numerical stability problems occur. This has also been recognized within the context of implicit integration by Borja *et al.* [5] and Rouainia and Muir Wood [6]. To avoid these numerical problems a minimum size ratio for the bubble of 0.12 was adopted. The relatively large size of the bubble is the reason why the adjustment of the curve for the smaller strains is not very good.

No matter how small, there is always, in both models, a purely elastic region having no damping at all. To avoid this, a small, 1% damping ratio of the Rayleigh type was used in all the analyses.

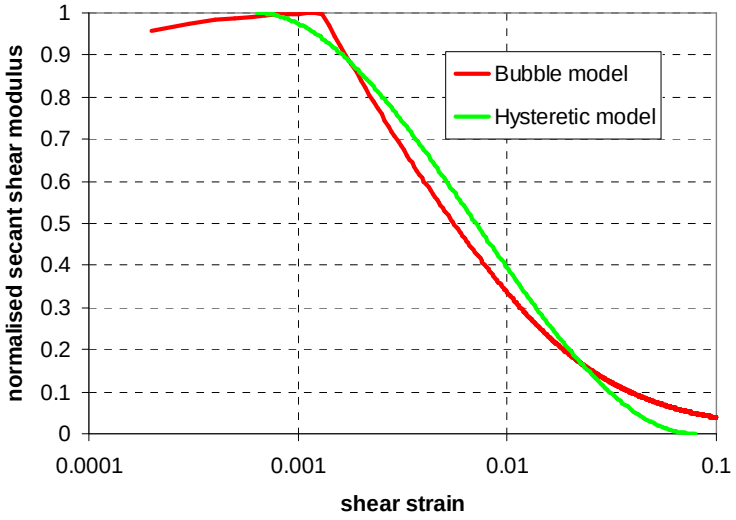

Figure 2: Modulus reduction curves for bubble and hysteretic models in a simple shear test.

3 THE INPUT SEISMIC ACTION

The seismic action adopted in this study is an acceleration history having the shape of a *sinus cardinalis* (sinc) function in the time domain (Figure 3). The function is defined as:

$$h(t) = \begin{cases} b\dfrac{\sin(a\,t)}{a\,t} & ;t \neq 0 \\ b & ;t = 0 \end{cases} \tag{3}$$

This function is associated with a constant spectral amplitude and a limited bandwidth, as shown in Figure 4. The parameter *b*, defines the amplitude of the signal and the parameter *a*, determines the maximum frequency present in the signal. As the bandwidth gets wider, the signal tends to a localized impulse (like as Dirac delta function). The advantage of this type of input signal is that, every frequency within given bounds has the same contribution. Because the shape of the input signal in the frequency domain is always flat, only the amplitude value *b* is needed to define it.

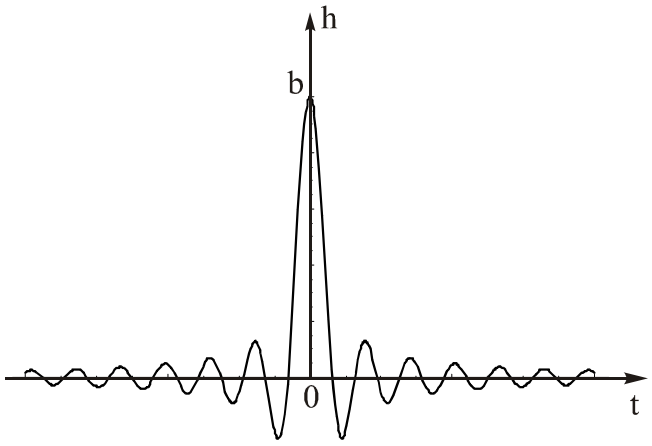

Figure 3: Input motion in the time domain.

In the present case, the input signal consists in a horizontal acceleration applied to the base of the model which acts as a rigid bedrock. The peak, *b*, values used were 0.5g, 1g and 2g. The duration of the action is 10s and the peak is attained after 5s. The maximum frequency applied is 20Hz.

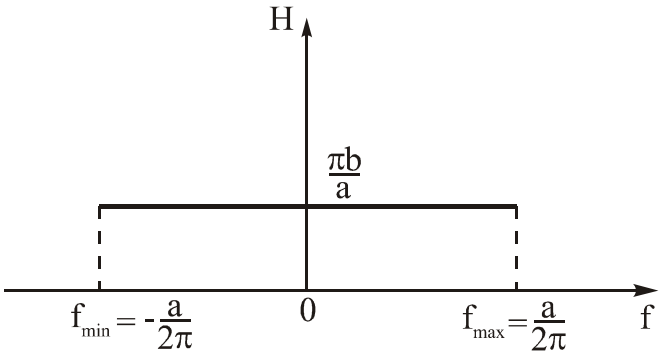

Figure 4: Input motion in the frequency domain.

4 MODEL OF THE TUNNEL

The case being analysed is a tunnel having a circular cross section with 10m diameter. The tunnel's crown is 10m below the ground surface. The ground where the tunnel is excavated is an overconsolidated hard clay. The soil is saturated and the water table is 2m below the ground surface. In the 2m above the water table negative pore pressures resulting from capillary forces were applied. The rigid bedrock is located at a depth of 46m. The numerical analyses are made with FLAC, under plane strain and undrained conditions. The mesh used in the analysis is shown in Figure 5.

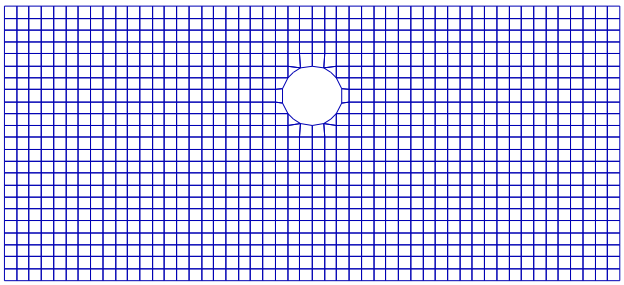

Figure 5: Mesh used in the numerical analyses.

Because the rigid base boundary has been adopted in the current model the input motions (horizontal acceleration) are applied to the model base. As regards the lateral boundaries free field conditions were applied. The initial stresses for the dynamic analyses, were taken from a single previous excavation analysis, including lining placement, made with the bubble model. This was the case for both the dynamic analyses made with the bubble model and the ones made with the hysteretic model. The procedures for simulating the excavation are described in detail in Maranha and Vieira [3]. The 0.25m thick linear elastic sprayed concrete lining (E=4.8MPa and ν=0.2), is applied after 30% stress relief. The seismic action is applied im-

mediately after construction, before any excess pore pressure dissipation takes place. Figure 6 shows the monitored points during all the performed analyses.

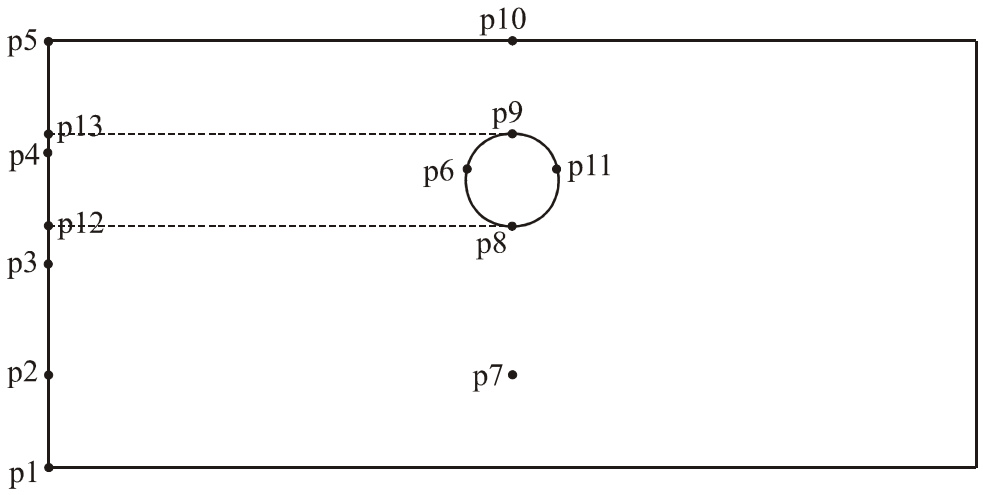

Figure 6: Location of history points.

5 ANALYSIS RESULTS

Before describing the results of the analyses, two important validation aspects were considered. The first aspect concerns the use of a mean effective stress dependent hypoelastic law incorporated in the bubble model as described in [3]. Because this hypoelastic law can generate energy in close stress and strain cycles, an evaluation of the consequences of this conceivable behaviour on the validity of the results must be made. To accomplish this evaluation, an analysis using a linear elastic law instead of the hypoelastic one with the bubble model, was performed using a 2g amplitude input. The initial shear and bulk moduli were the ones obtained from the hypoelastic law at the end of the construction stage. The rather small differences in the results relative to the analysis using the hypoelastic model confirm that, in this case, the non-conservative behaviour of the model does not invalidate the results obtained.

Another aspect evaluated was the actual performance of the free field boundary conditions used. This was done by comparing the results of a single column analysis, having one element width, using free field lateral boundary conditions with the results at the free field boundary of the tunnel analysis. The results were almost the same.

5.1 Spectral acceleration amplification ratio

Input acceleration signals, defining the horizontal shear wave, having maximum amplitudes of 0.5g, 1g and 2g, where analysed. The highest frequency in all cases was 20Hz. For each one of the amplitudes two analyses were performed, using both the bubble continuous plasticity model and the hysteretic model described above.

The natural frequencies of the soil layer were computed using an analytical solution, due to Ambraseys [7] that assumes the soil to be linear elastic with the shear modulus increasing linearly with depth. The natural frequencies are obtained from

$$f_n = \frac{a_n(1-K^2)v_s^0}{4\pi H\, K} \tag{4}$$

where $K = \sqrt{G_0 / G_H}$, H is the thickness of the soil layer, $v_s^0 = \sqrt{G_0 / \rho}$, G_0 and G_H are, respectively, the shear modulus at the top and the bottom of the layer, and a_n is the n*th* root of the equation

$$J_0(a_n)Y_1(K\,a_n) - J_1(K\,a_n)Y_0(a_n) = 0 \tag{5}$$

The displacement patterns for the standing waves (mode shapes) corresponding to the natural frequencies are obtained from

$$u_n(z) = J_0\left(a_n\sqrt{\frac{1+f\,z}{1+f\,H}}\right)Y_0(a_n) - Y_0\left(a_n\sqrt{\frac{1+f\,z}{1+f\,H}}\right)J_0(a_n) \tag{6}$$

with $f = (G_H - G_0)/(G_0\,H)$.

The first five natural frequencies, computed from the numerical analyses, can clearly be seen in the spectral amplification ratio plot at point 5, for an input signal with 0.5g amplitude, as presented in Figure 7. In this case, where the amplitude of signal is smaller, the response is closer to the linear elastic one. The response of both models is very similar. The analytical values for the natural frequencies are quite near (within 6%) the computed values. The analytical value for the fundamental frequency (0.64Hz) deviates only 1% of the computed value. As expected, amplification ratios decrease with increasing frequency.

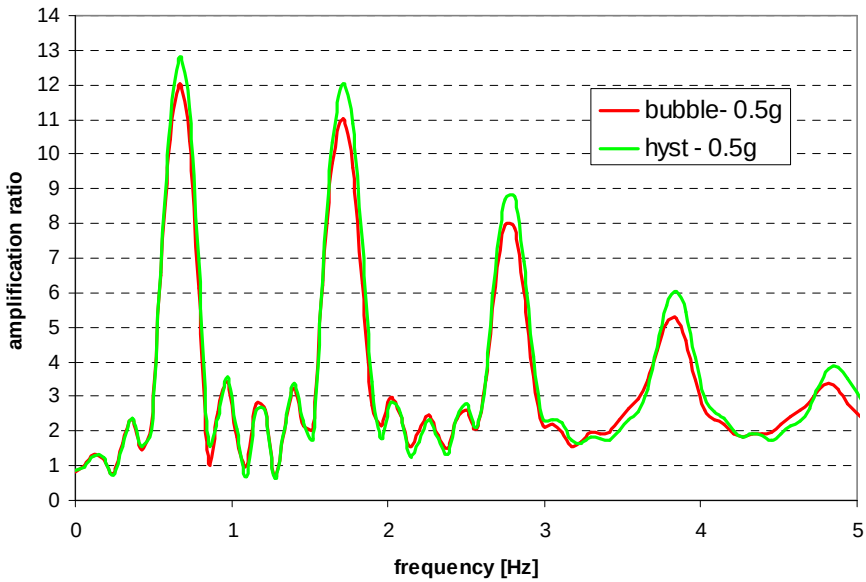

Figure 7: Spectral amplification ratio at point 5, for bubble and hysteretic models (0.5g).

Considering point 4, which is located on the free field at a depth of 12m, it can be observed in Figure 8 that the second natural frequency is suppressed. This is due to the point being located in close proximity to a nodal point (zero horizontal displacement) of the second vibration mode. Point 3 is located on the free field at 24m depth and is close to a nodal point of the

third mode. This explains the suppression of the third mode that can be observed in Figure 9. This nodal point effect is also present at 1g and 2g input amplitude levels.

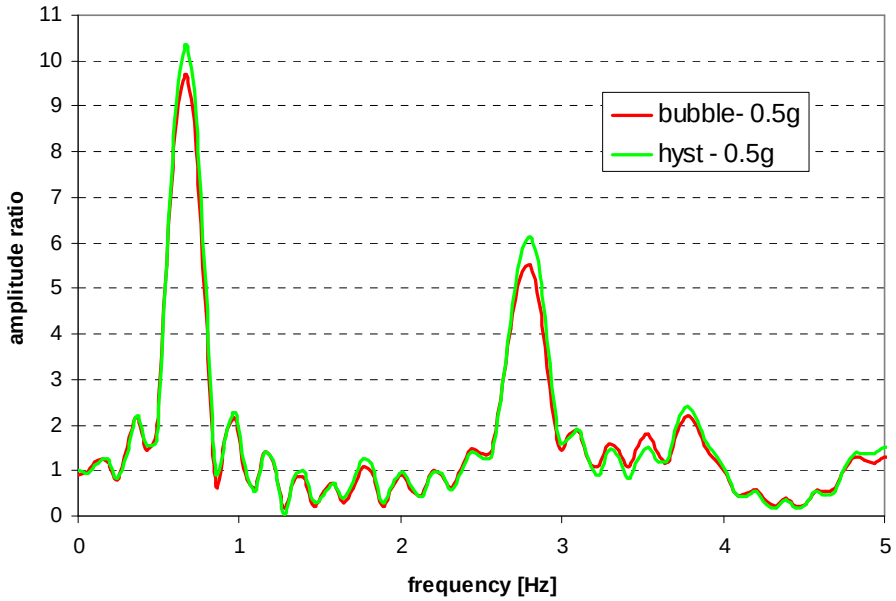

Figure 8: Spectral amplification ratio at point 4, for bubble and hysteretic models (0.5g).

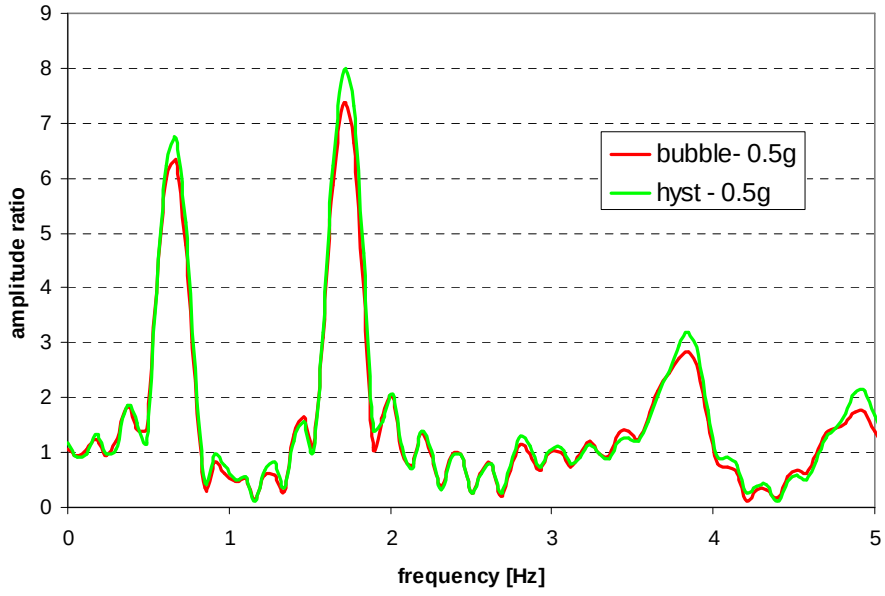

Figure 9: Spectral amplification ratio at point 3, for bubble and hysteretic models (0.5g).

In Figure 10, the spectral acceleration amplification ratio is plotted at point 5, located at the surface on the free field, for both models and 0.5g and 2g input amplitude levels. It is apparent that, when increasing the amplitude level from 0.5g to 2g, the bubble model originates

much reduced amplification ratios while, in the case of hysteretic model, they remain essentially the same. The damping produced by the bubble model increases with the amplitude of the input signal. This does not occur with the hysteretic model.

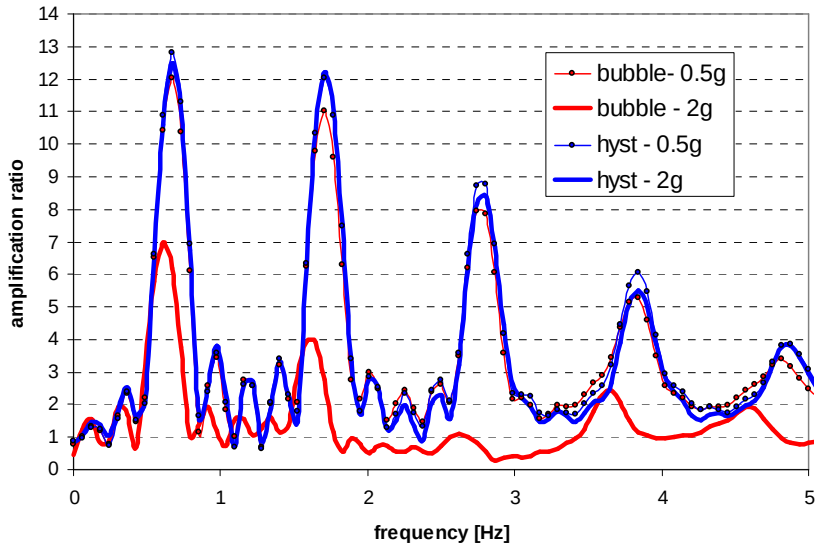

Figure 10: Spectral amplification ratio at point 5, for both models (0.5g and 2g).

In order to evaluate the tunnel effect, the response of points on the free field is compared with that of point at the same depth but horizontally aligned with the tunnel's axis. In Figure 11, the amplification ratio for point 5, at the ground surface, on the free field, is compared with that of point 10, at the surface, above the tunnel's axis. The input amplitude is 2g. The point aligned with the tunnel produces significantly lower amplification ratios, for frequencies higher than the fundamental one, than the point on the free field. This effect, although less pronounced than at surface level, also takes place at other depths.

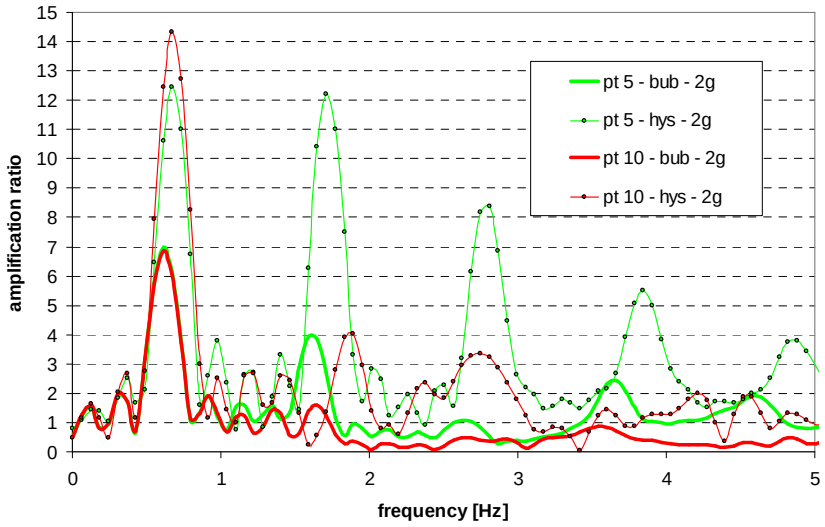

Figure 11: Spectral amplification ratio at points 5 and 10, for both models (2g).

5.2 Stress-strain behaviour

The curves of shear stress variation with shear strain, computed at an element situated directly above the tunnel's crown, are plotted in Figure 12. Both models as well as three input amplitude levels (0.5g, 1g and 2g) are represented. At the lower amplitude level, 0.5g, the response is similar between both models. At 2g, there is a divergent response between the models, with the hysteretic model displaying larger and more open loops.

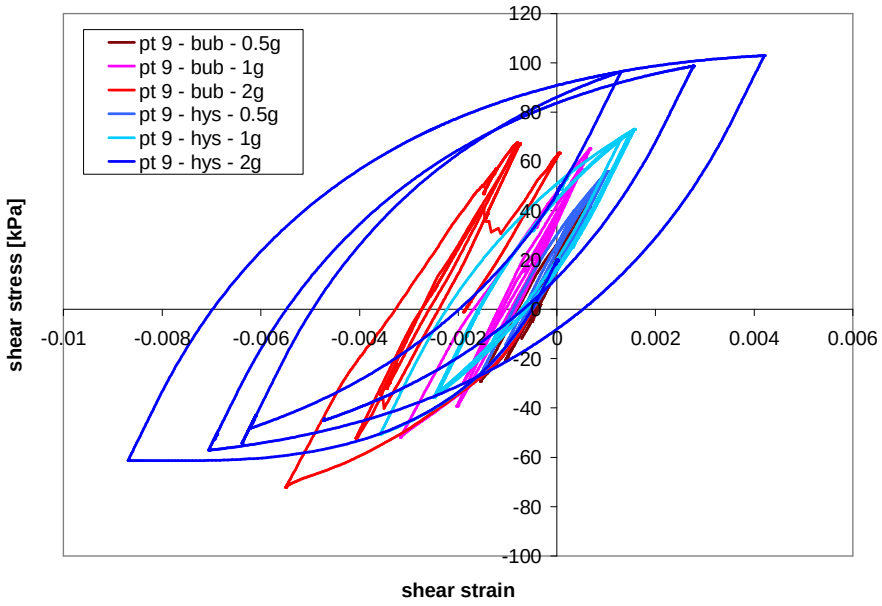

Figure 12: Shear stress vs shear strain at point 9. Bubble and hysteretic models. (0.5g, 1g, 2g).

5.3 Pore pressure time histories

Figure 13 shows the pore pressure time histories obtained at the monitored point 1, located at the bottom of the soil layer, and at point 9, above the tunnel's crown, for both models. The input amplitude used is 2g. There is a qualitative difference between the pore pressure response given by each of the models. Because it incorporates dilatancy, the bounding surface bubble model can generate excess pore pressures with each cycle of loading. At point 1, there is a significant increase in pore pressure that persists despite the loading cycles. Here the soil is in the contractant region. At point 9, the soil is in the dilatant region and there is a continuous decrease in the pore pressure, which eventually becomes lower than the atmospheric pressure. At about 9.5s, the pore pressure reaches the fluid tension limit and there is cavitation (the pore pressure becomes equal to the atmospheric pressure). The hysteretic model exhibits independence between volumetric and distortional behaviour and, as such, cannot reproduce dilatancy. The pore pressure variations arise solely due to corresponding variations in the mean effective stress. For this model, both at points 1 and 9, it is observed that after each loading cycle, no excess pore pressure remains.

The difference in pore pressure response between the models also helps to explain the disparity observed in the shear stress-strain curves at point 9. Due to the suctions that were generated by the bubble model, the mean effective stress is higher and, consequently, the stiffness is also higher than is the case for the hysteretic model.

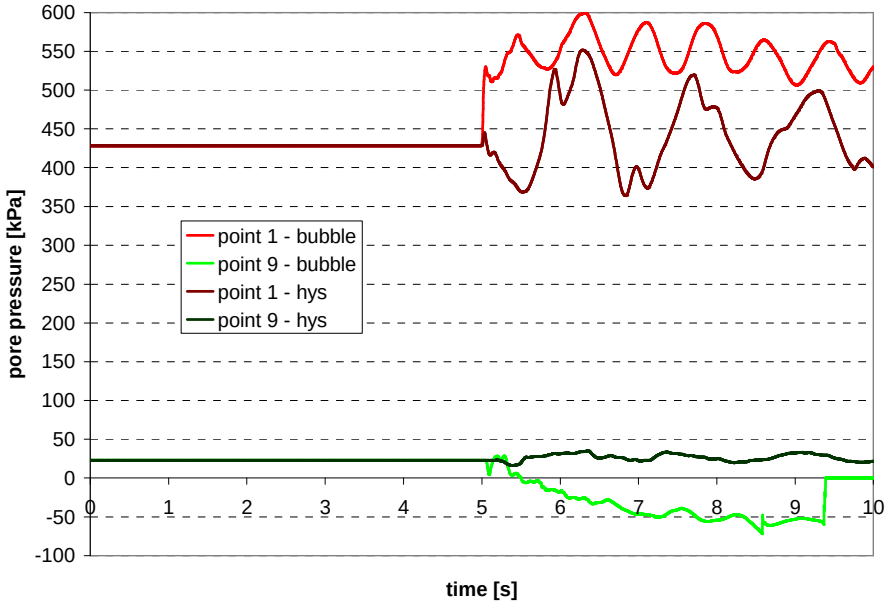

Figure 13: Pore pressure histories at points 1 and 9, for bubble and hysteretic models (2g).

5.4 Tunnel displacements

The relative horizontal displacement between the crown and the invert of the tunnel (crown minus invert) is a measure of the tunnel's shearing. When compared with the relative horizontal displacement of points at the same level but located on the free field, it can be used to assess the effect of interaction with the tunnel. The relative horizontal displacements between points 8 and 9 (tunnel), and between points 13 and 12 (free field), are plotted in Figure 14 for an input amplitude of 2g. The interaction effect is not apparent in the bubble's model instance – the relative displacements are almost the same on the tunnel and on the free field. This is not the case with the hysteretic model, where the distortion level in the tunnel is higher than in the free field. Also, the maximum relative displacement, for the bubble model, has a value of 7cm and occurs immediately after the main shock, while in the case of the hysteretic model, it has a value of 8cm and takes place only 3.5s after the shock, during the third cycle.

6 CONCLUSIONS

Nonlinear dynamic numerical analyses of a tunnel, excavated in overconsolidated hard clay, under the action of a bandwidth limited (max. 20Hz) acceleration history having a constant value in the frequency domain, were accomplished. A bounding surface type model with a bubble that accounts for plastic anisotropy as well as a simpler variable elasticity, hysteretic model were used to model the soil behaviour. Three levels of input acceleration amplitude were considered (0.5g, 1g and 2g). The interpretation of the results leads to the following main conclusions:

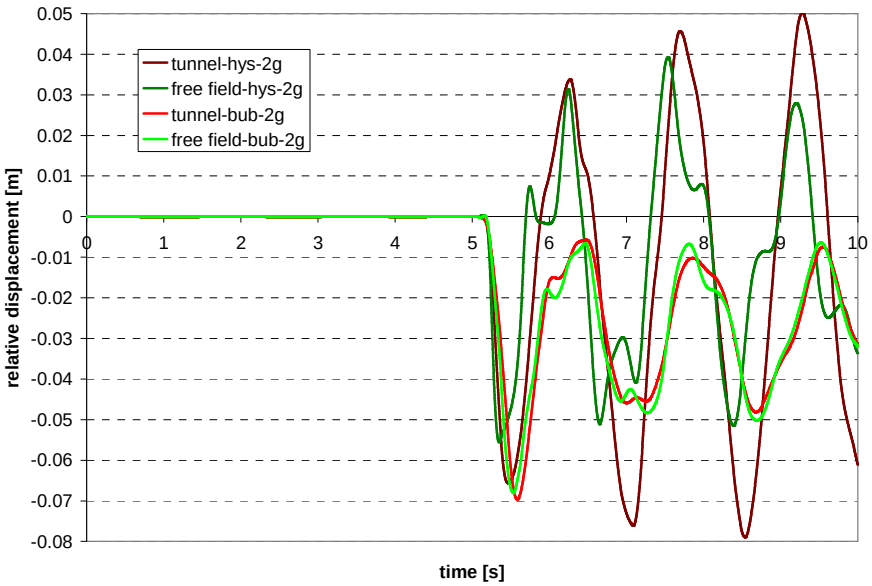

Figure 14: Relative horizontal displacements on the tunnel (crown minus invert) and free field (2g).

1) As expected, natural frequencies computed from the analytical solution for a soil layer with linearly varying shear modulus agree well with those observed in the numerical analyses for the lower input amplitude level (0.5g).

2) The suppression of some natural frequencies at points located at some specific depths is explained by the proximity of those points to nodes in modal shapes associated with the suppressed natural frequencies.

3) As expected, for the lower input amplitude level (0.5g), the response of both models is very similar, given that the soil behaviour is approximately linear elastic.

4) The damping produced by the bubble model increases significantly with the amplitude of the input signal. This does not occur with the hysteretic model.

5) The points vertically aligned with the tunnel's axis show a reduction in the amplification when compared with points at the same depth on the free field. This is particularly evident at the surface.

6) In terms of shear stress versus shear strain curves, it is observed that, while the response is similar between the models for the lowest input amplitude, it diverges significantly for the highest one.

7) The computed pore pressure changes generated by both models differ significantly due to the lack of capability of the hysteretic model to reproduce dilatant soil behaviour in contrast with what happens with the bubble model.

8) Relative horizontal displacements between the crown and the invert of the tunnel, when compared with the free field corresponding displacements, show that the interaction with the tunnel is negligible in the case of the bubble model.

REFERENCES

[1] Kavvadas M., Belokas G. 2001. An anisotropic elastoplastic constitutive model for natural soils. In: Desai et al. (eds) Computer Methods and Advances in Geomechanics, Balkema, Rotterdam, pp 335-340.

[2] Dafalias Y.F. 1986. Bounding surface plasticity. I: mathematical foundation and hypoplasticity. *Journal of Engineering Mechanics*, 112: 966-987.

[3] Maranha, J. R., Vieira, A. 2008. Influence of initial plastic anisotropy of overconsolidated clays on ground behaviour during tunneling. *Acta Geotechnica*, 3: 259-271.

[4] Kavvadas M., Amorosi A. 2000. A constitutive model for structured soils. *Geotechnique*, 50: 263-273.

[5] Borja, R. I., Lin, C. H., Montáns, F. J. 2001. Cam-Clay plasticity, Part IV: Implicit integration of anisotropic bonding surface model with nonlinear hyperelasticity and ellipsoidal loading function. *Computer Methods in Applied Mechanics and Engineering*, 190: 3293-3323.

[6] Rouainia, M., Muir Wood, D. 2001. Implicit numerical integration for a kinematic hardening soil model. *International Journal for Numerical and Analytical Methods in Geomechanics*, 25: 1305-1325.

[7] Ambraseys, N. N. 1959. A note on the response of an elastic overburden of varying rigidity to an arbitrary ground motion. *Bulletin of the Seismological Society of America*, 49: 211-220.